Optical Study of Semiconducting Non-Molecular Nitrogen Under Pressure

E. Gregoryanz, A. Goncharov, R. Hemley, I Liu, H. Mao
Geophysical Laboratory, Carnegie Institute of Washington, Washington, D.C.

A number of molecular solids are known to undergo a transition to a nonmolecular (NM) phase under high compression (e.g. iodine [1], hydrogen halides [2] and ice [3]), which could be accompanied by an insulator-to-metal transition. In this regard, nitrogen is considered a model system, as it is one of the most strongly bonded molecules and is expected to undergo the NM transition (destabilization of its triple bond) in the pressure range accessible by modern experimental techniques. This prediction is based on the results of shock-wave experiments, which provided evidence for the NM transition in the liquid phase at 30 GPa and 6000 K [4], as well as theoretical calculations for the solid [5-7]. The latter predictions involved transitions to various three-fold coordinated phases below 100 GPa. It has been suggested that the observed transition pressure can be substantially higher because of a large potential barrier to dissociation (*e.g.* Refs. 6 and 7).

Raman measurements of nitrogen have been carried out to 130 GPa [8] and 180 GPa [9]. The lowest-frequency vibron has been observed in both studies to the highest pressure reached, and the persistence of this vibron was interpreted as the existence of a molecular phase to those pressures. Also, visual observations [8,9] and visible transmission measurements in Ref. 8 reveal color changes at 130-180 Gpa, but no quantitative characterization has been done. Here, we report the results of a combined study of the optical and vibrational properties of N_2 by visible and IR spectroscopy, and Raman scattering done with new techniques [10], including synchrotron IR spectroscopy and Raman spectroscopy with near IR excitation. We present evidence for the NM transformation in the 140-160 GPa range to a disordered, single-bonded, three-fold-coordinated structure.

Six separate high-pressure experiments with a Mao-Bell diamond anvil cell have been performed at room temperature with the maximum pressures reached varied from 180 to 268 GPa. Details of our IR/Raman setup at beamline U2A at the NSLS are published elsewhere [10]. Beyond the pressure of 130 GPa, excitations in the 693-750 nm range from a Ti:sapphire laser were used for both Raman and ruby luminescence measurements to avoid strong sample and diamond fluorescence, as well as premature diamond failure.

Raman spectra to 140 GPa reveal an abundance of vibrational modes in agreement with previously reported results [8,11-13]. At moderate pressures, our data are in agreement with those reported in Refs. 11, 8 and 13. We find a monotonic increase in frequency of all lattice modes and redistribution of their intensities with pressure, so that high frequency bands dominate at the highest pressures. As in Refs. 8,12 and 13, we observe branching of the Raman-active vibrons at around 90 GPa followed by an increase in their frequency separation. Intensity redistribution is also observed as the lowest frequency vibron ν_2 gathers most of the intensity at the highest pressures.

IR absorption spectra reveal a multiplet of modes in the vibron spectral range and also a newly discovered mode of lattice vibrations (Fig. 1). The pressure dependencies of IR vibron frequencies match well the extrapolation of the lower pressure data reported in Refs. 14 and 15. The pressure dependence of the lattice mode frequency is very close to that of the highest frequency Raman lattice mode(Fig. 1a). As in the case of Raman vibrons, the IR vibrons show branching with pressure, so that up to 5 vibrons can be observed at high pressure, all of which originate from the ν_2 multiplet. The Raman and IR vibrons probe different points of the large Brillouin zone and become accessible because of its folding. According to Ref. 13, the lowest-frequency Raman vibron corresponds to the lowest frequency of the Brillouin zone and represents the case where all molecules on the faces of the unit cell vibrate in phase. The other vibrons (Raman and IR) involve different out-of-phase vibrations and form a compact group close to the frequency of the uncoupled N-N stretch. The Raman and IR vibrons lose their intensities in the 140-160 GPa pressure range and completely disappear at higher pressures. No substantial change in linewidth was observed prior to disappearance of the vibrational features, so this effect cannot be due to pressure gradients. This is also observed for the Raman and IR lattice modes. It may be argued that the disappearance of the Raman modes is attributed to the presence of a luminescence background (quite moderate with red excitation) and an increase of the visible sample absorption (see below). However, IR intensities are totally independent of these factors because the sample remained transparent in the mid-IR spectral range.

Fig. 2 presents the results of visible and IR absorption measurements of nitrogen at elevated pressures. Below 140 Gpa, nitrogen is transparent in the entire

measured spectral range (600-20000 cm^{-1}) except the absorption on relatively weak vibrational excitations. At 150 Gpa, a wide absorption edge appears in the visible part of the spectrum (Fig. 2a), at which point the sample becomes yellow, and then totally opaque (inset of Fig. 2) at 160 GPa. This transformation substantially affected the measurement of IR spectra because of increased absorption in the near-IR range. Nevertheless, we measured IR absorption spectra to the highest pressure reached in the experiment (about 170 GPa). Inspecting the spectra at different pressures above 150 GPa one can easily infer that, to a first approximation, they can be obtained by simple scaling, indicating an increase of the abundance of the new phase with increasing pressure. This matches closely the vibrational spectroscopic observations of a gradual disappearance of all excitations in the molecular phase (see above) between 140 and 170 GPa. The Raman and IR spectra of the new phase show a rather broad, weak Raman band at 640 cm^{-1} as well as a broader IR band at 1450 cm^{-1} (Fig. 3). Their intensities seem to increase gradually with pressure, concomitant with a decrease in the intensity of molecular excitations, implying the coexistence of two phases between 140 GPa and 170 GPa.

The complete change in vibrational excitations and appearance of the low-energy band gap provide evidence for the transformation from the molecular phase to a nonmolecular phase with a narrow gap. Theoreti-

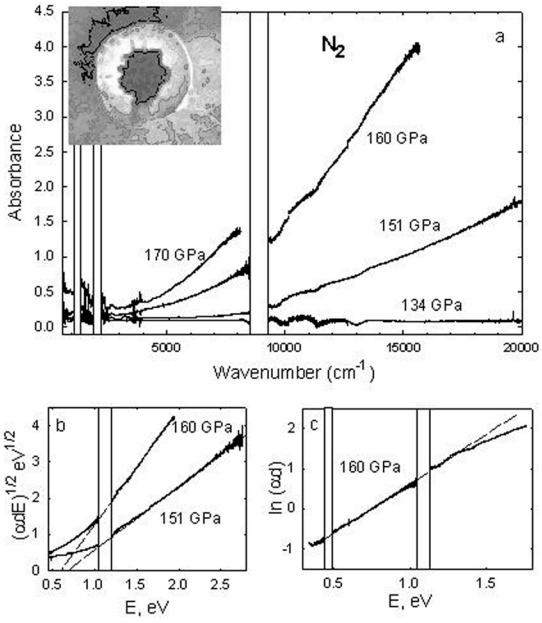

Fig. 2 (a) Optical absorption spectra in a wide spectral range at different pressures [Inset: the microphotograph of the opaque sample at 160 GPa]. (b) Absorption data at 151 and 160 GPa illustrating a direct allowed gap absorption law at high energies. (c) Absorption data at 160 GPa illustrating an Urbach-like absorption law at low energies.

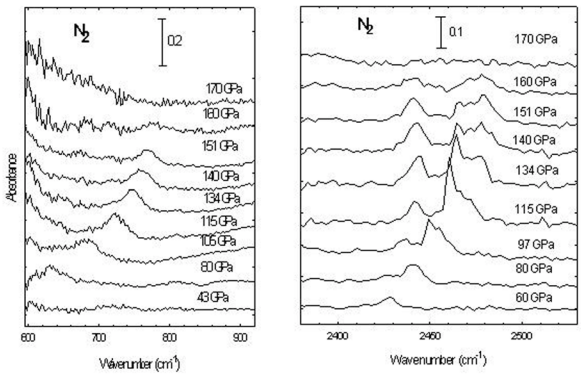

Fig. 1 IR absorption spectra in the 80-170 GPa range at 300 K. Left panel: lattice vibrations. Right panel: vibrons (points: experiment, solid lines: phenomenological fit, dotted lines: individual bands).

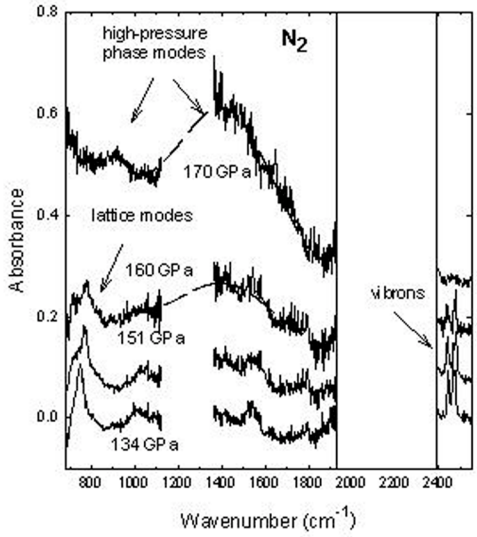

Fig 3. IR absorption data in the vibrational spectral range through the transition. No data could be obtained in the 1120-1370 cm-1 and 1920-2380 cm-1 spectral ranges because of strong absorption by the diamonds.

cal calculations predict a transformation to threefold-coordinated cubic or distorted cubic structures [5-7] associated with a substantial volume discontinuity (25-33%).

The analysis of the shape of the absorption edge of the high-pressure phase (Fig. 2a) shows the existence of two spectral ranges with different types of energy dependence on the absorption coefficient. At high values of absorption it follows the empirical Tauc relation [16] in the case of parabolic band edges (Fig. 2b), while at smaller absorption a so-called Urbach or exponential absorption tail [17,18] is observed (Fig. 2c). The existence of this kind of absorption edge is normally related to amorphous semiconductors. Absorption data at 151 and 160 Gpa, plotted in photon energy E versus $(\alpha dE)^{1/2}$ (α-absorption coefficient, d-sample thickness) coordinates, illustrate a direct allowed gap absorption law at high energies. Extrapolations of those dependencies to zero absorption give an estimate of the direct gap value. We observe a monotonic red shift of the band gap with pressure up to the highest pressure reached (268 Gpa). Linear extrapolation of the gap values to higher pressures predicts the metallization by the band gap closure at above 280 GPa. This should be considered as a lower limit unless an unexpected phase transition occurs in this pressure range.

The converging agreement of the recent results for nitrogen using synchrotron IR, Raman, optical [19] and electrical transport measurements [20] demonstrate the accuracy of the new high pressure techniques.

Acknowledgements

This work was supported by NSF and NSLS.

References

[1] K. Takemura, S. Minomura, O. Shimomura, and Y. Fujii, Phys. Rev. Lett., **45**, 1881, 1980.
[2] E. Katoh et al., Phys. Rev. B. 61, 119, 2000; E. Katoh et al., Phys. Rev. B., **59**, 11244, 1999.
[3] A. Goncharov et al., Science, **272**, 149, 1996; K. Aoki, H. Yamawaki, M. Sakashita, and H.Fukihisa, Phys. Rev. B, **54**, 15673, 1996; A. Goncharov, V. Struzhkin, H. Mao, and R. Hemley, Phys. Rev. Lett., **83**, 1998, 1999.
[4] H. Radousky et al., Phys. Rev. Lett., **57**, 2419, 1986.
[5] A. McMahan and R. LeSar, Phys. Rev. Lett., **54**, 1929, 1985.
[6] R. Martin and R. Needs, Phys. Rev. B, **34**, 5082,1986.
[7] C. Mailhiot, L. Yang, and A. McMahan, Phys. Rev. B, **46**, 14419, 1992.
[8] R. Reichlin, et al., Phys. Rev. Lett., **55**, 1464, 1985.
[9] P. Bell, H. Mao, R. Hemley, Physica, **139&140B**, 16, 1986; R. Hemley (unpublished data)
[10] A. Goncharov et al. in: Science and Technology of High Pressure, Eds: M. Manghnani, W. Nellis, M. Nicol, Vol. **1**, p.90, Universities Press, Hyderabad India, Honolulu Hawaii, 2000.
[11] D. Schiferl, S. Buchsbaum and R. Mills, J. Chem. Phys., **89**, 2324, 1985.
[12] H. Olijnyk and A. P. Jephcoat, Phys. Rev. Lett., **83**, 332, 1999.
[13] H. Schneider, W. Hafner, A. Wokaun, and H. Olijnyk, J. Chem. Phys., **96**, 8046, 1992.
[14] M. D. McCluskey, L. Hsu, L. Wang, and E. E. Haller, Phys. Rev. B, **54**, 8962, 1996.
[15] R. Bini, M. Jordan, L. Ulivi, H. J. Jodl, J. Chem. Phys., **106**, 6849, 1998.
[16] J. Tauc, R. Grigorovici, and A. Vancu, Phys. Status Solidi, **15**, 627, 1966.
[17] F. Urbach, Phys Rev., **92**, 1324, 1953.
[18] N. F. Mott and E. A. Davis, Electronic Processes in Non-Crystalline Materials, 2nd Ed., Clarendon Press, Oxford (1979).
[19] A. Goncharov, E. Gregoryanz, H. Mao, Z. Liu and H. Hemley, Phys. Rev. Lett., 1262, **85**, 2000.
[20] M. Eremets, R. Hemley, H. Mao and E. Gregoryanz, Nature (submitted).

Quantum Dots in Dendrimer Templates – Small Angle X-ray Scattering Allows Characterization of New Nanoparticles with Promising Properties

F. Gröhn, B.J. Bauer and E.J. Amis

Polymers Division, National Institute of Standards and Technology, Gaithersburg, Maryland

Quantum-size effects cause inorganic particles of nanometer size to have unique optical, electrical and magnetic properties that characteristically depend on their size and shape, and can lead to a wide variety of practical applications. On the other hand, organic compounds - and polymers in particular - often have advantageous mechanical properties, can self-assemble into ordered structures and can be functionalized via chemical modification. Therefore, it is expected that hybrid inorganic-organic structures with characteristic nanometer length scales will yield special materials with promising property combinations. While such organic-

inorganic hybrid nanostructures can be found in natural materials quite often, e.g. in sea shells or bone, the synthetic design of hybrid nanostructures has only recently come into focus.

Polymer nanotemplating is one approach to synthesize organic-inorganic hybrid nanostructures. An inorganic crystal is nucleated within a polymeric matrix and the growth is controlled by features of this matrix, such as elasticity or charges, in addition to the usual factors such as free energy of crystal formation and surface tension.[1]

In order to take advantage of such approaches, it is necessary to understand the formation of hybrid structures. Dendrimers, organic molecules with a size of 1 to 15 nm, serve here as a mesoscopic model system ranging from typical organic low molecular mass molecules to typical polymers. Dendrimers are monodisperse and double in molecular mass for successive generations (labeled G*n*, *n*=2-10 hereafter). The shape of dendrimers changes from star-like (G2-G4) to homogeneous spheres (G8-G10).[2]

In our templating approach, polyamidoamine dendrimers in aqueous solution attract precursor metal ions due to their opposite charge, or complexation to dendrimer amine groups. In a second step, chemical reactions, e.g. the reduction of gold ions to gold metal, can produce colloid structures that are controlled by the dendrimer.[3]

Small-angle x-ray scattering (SAXS) is a powerful technique to investigate such hybrid nanostructures. Figure 1a shows scattering data of hybrid structures with ”low generation” and “high generation” dendrimers as potential templates. To analyze the data, we Fourier transformed the experimental scattering curves I(q) into pair distance distribution functions P(r) using the indirect transformation methods developed by O. Glatter. Figure 1b is a schematic of the hybrid particle formation derived from the SAXS results.

Multiple lower generation dendrimers associate with the inorganic colloid to form large aggregated hybrid structures. These observations are confirmed by transmission electron microscopy and small-angle neutron scattering experiments. Apparently, several dendrimers attach to the surface of a growing colloidal crystal, as is the case in the classical colloid stabilization by low molecular mass molecules.

Different results are obtained with higher generation dendrimers: Gold particles are formed inside individual dendrimer molecules. For G7 to G9, single nanoparticles are formed corresponding to the number of precursor ions added per dendrimer. We refer to this mechanism as the “fixed loading law.”[3] For example, 2.5 nm, 3.5 nm and 4.2 nm particles within G7, G8 and G9 dendrimers are observed, corresponding to about 512, 1024 and 2048 atoms. For these generations, the dendrimer controls the size of the nanocluster.

For G10, multiple smaller particles are formed instead. To understand this, one has to consider that the growth of a nucleated colloid is limited by the finite extension of neighbouring polymer chains. With each generation number the mass of the dendrimer is roughly doubled, while the size increases only linearly, i.e., as the generation number increases, the internal dendrimer segment density increases and the flexibility of the dendrimer chains decreases. Thus, there is a limit to colloid growth. For the G10 dendrimer the chain flexibility is insufficient to allow for the growth of a single colloidal particle. On the other hand, the increased surface to be stabilized for multiple smaller particles is likely to be provided by the G10 dendrimer. Interestingly, the “fixed loading” seems to be still valid (4096 atoms). The G10 dendrimer still realizes a host-guest nanotemplating and the changed dendrimer structure results in a different colloid morphology.

Thus, we have observed a transition in stabilizing mechanism from a typical colloid stabilization (G2-G4) to polymer nanotemplating (G7-G10) with increasing dendrimer generation, i.e. increased molecular mass but unchanged chemistry (see Figure 2). This can be understood from the dendrimer structure itself, which changes with increasing dendrimer generation from a star-like molecule to a “polymeric” homogeneous sphere.[3]

Semiconductor quantum dots represent a different class of colloids with high potential for novel applications. We have also used the host-guest nanoscale synthesis with dendrimers to produce CdS and CdSe nanocrystals. Due to quantum size effects, these species show a strong fluorescence. Figure 3 shows diluted solutions of CdS-dendrimer hybrid particles upon excitation with UV light. The color of the fluorescence indicates the change in particle size with dendrimer generation and the accompanying change in stabilizing mechanism.

Semiconductor quantum dots are excellent materials for potential nanoscale optoelectronic devices and biosensors. Due to the high photostability and size dependent fluorescence color, nanocrystals have a high potential as fluorescent probes in diagnostic labeling. In contrast to previous synthetic methods, the number of atoms forming one “quantum dot” is controlled with the dendrimeric template. These particles can be dissolved in water and dendrimer amine groups can be used to attach certain “functions.”

Dendrimer nanotemplating has thus been proven to be an effective method for the controlled design of promising hybrid particles, which were characterized by synchrotron small-angle x-ray scattering. Furthermore, we note that the approach described here can

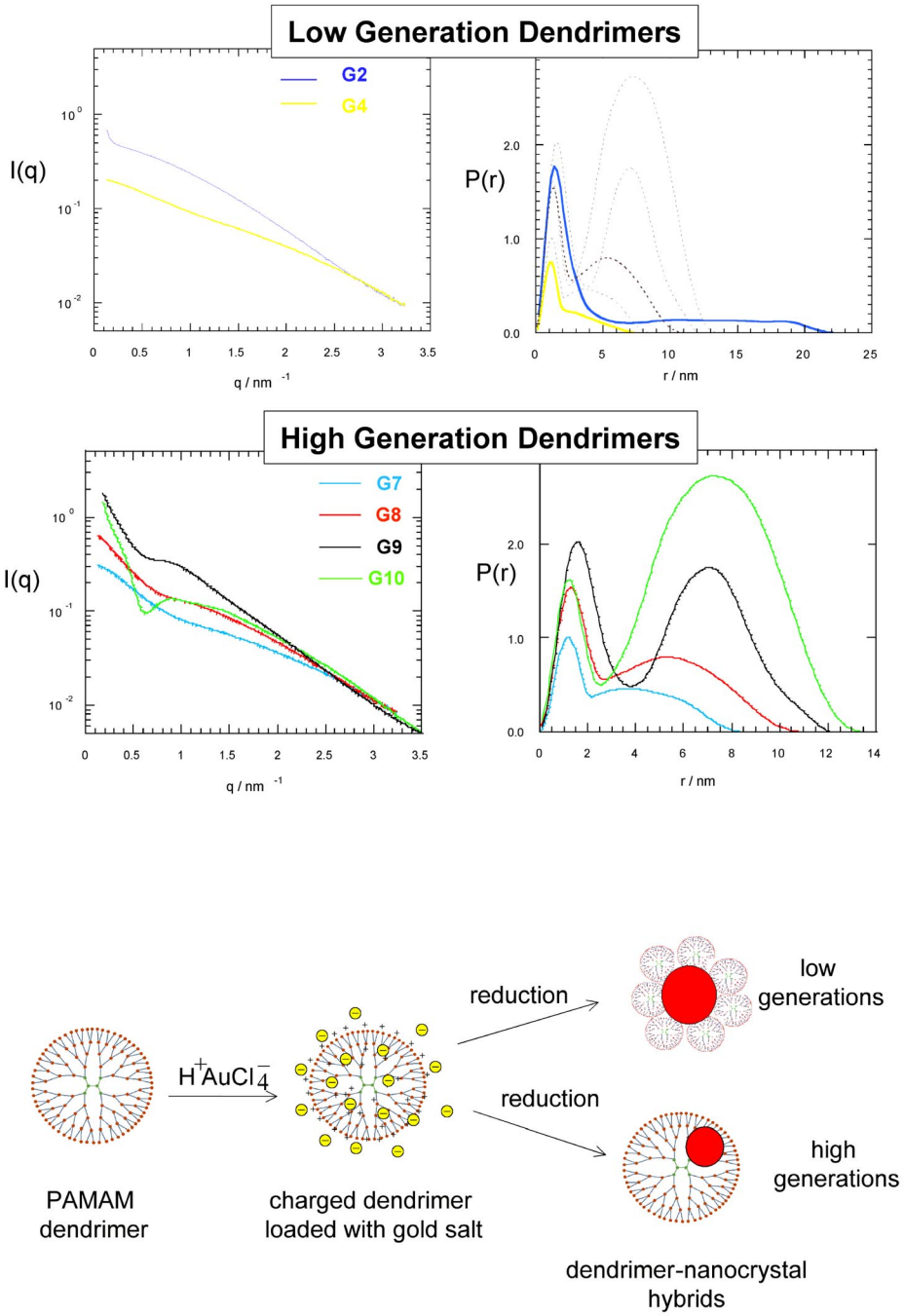

Figure 1. Small-angle x-ray scattering of dendrimer nanotemplating in aqueous solution in dependence of dendrimer generation. ***(a)*** *Scattering curves I(q), and pair distance distribution functions P(r), for low generation dendrimers and high generation dendrimers.[4]* ***(b)*** *Schematic of the hybrid particle formation.*

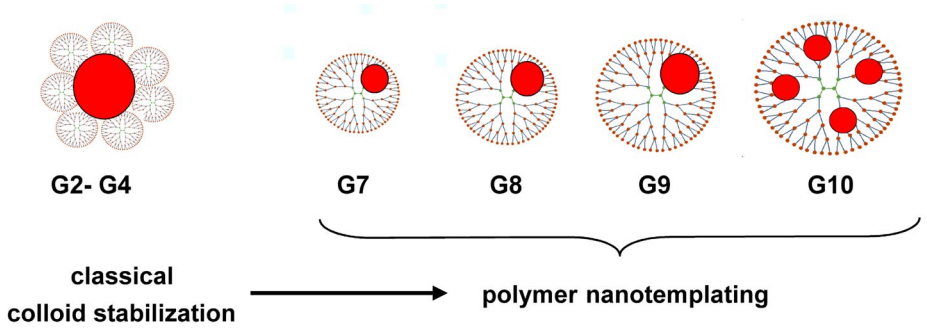

Figure 2: Change of stabilizing mechanism with dendrimer generation: Cartoons of resulting hybrid particles.

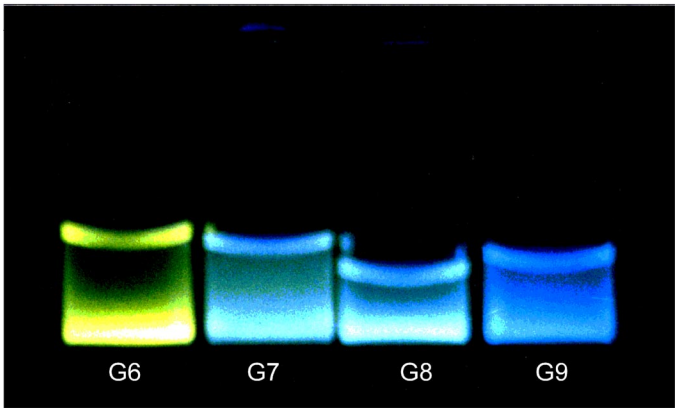

Figure 3: Photograph of solutions of CdS-dendrimer hybrid particles upon illumination with a hand-held UV-lamp: The change of stabilizing mechanism becomes evident from the color of the fluorescence.

be transferred to solid polymeric materials (see this report, abstracts from beamline X27C).

Acknowledgments:

We gratefully thank Profs. Ben Chu and Ben Hsiao and Drs. Fengi Yeh and Lizhi Liu for their kind support during the experiments at beamline X27C. We thank Dr. Donald Tomalia of MMI for providing us with dendrimers and Dr. Brent Viers for discussions. This work is supported in part by the U.S. Army Research office under contract number 35109-CH. We especially thank the Brookhaven Center for continuous essential support!

References:

1. M. Antonietti, F. Gröhn, J. Hartmann, L. Bronstein, Angew. Chem Int. Eng. Ed., *36*, 2080, 1997.
2. T.J. Prosa, B.J.Bauer, E.J. Amis, D.A. Tomalia, R. Scherrenberg, J. Polym. Sci., *35*, 2913, 1997. (also a study from beamline X27C at NSLS)
3. F. Gröhn, , B.J. Bauer, Y.A. Akpalu, C.L. Jackson, E.J. Amis, E.J.; Macromolecules, *33*, 6042, 2000 and references therein. See also: Science Highlight, Chemical Sciences, NSLS Activity Report 1999.
4. Error bars (measured standard deviation in I(q) and standard deviation in the estimation of P(r), which results from the fit to the I(q) data, respectively) are within the thickness of the plotted lines.